Scientia Iranica, Vol. 11, Nos. 1&2, pp 26–36

SCIENTIA
IRANICA

Aeroelastic Analysis of Guided Hypersonic Launch Vehicles

S.H. Pourtakdoust* **and N. Assadian**[1]

This study is concerned with the general motion of a guided flexible launch vehicle idealized as a non-uniform beam under continuous thrust action. The governing equations of motion are derived following the Lagrangian approach and generalized coordinates. The rigid motion consists of the conventional vehicle velocities (rotational and translative), whereas the elastic motion, introduced through modal substitution, represents the vehicle local lateral and transverse displacements relative to a mean body axis system. A complete simulation routine has been developed, which allows for investigation of the influence of various vibrational forcing functions, local stiffness changes and the Inertial Measurement Unit (IMU) displacements on the vehicle trajectory and the required control action histories.

INTRODUCTION

Dynamic and aeroelastic analysis of flying vehicles has usually been considered on the basis of rigid body motion and a few independent elastic degrees of freedom [1,2]. Consequently, the interaction effects of elastic modes on rigid motion will remain unrealizable [2]. This approach could yield acceptable error levels, as long as the structure under study is sufficiently stiff. However, for flexible high fineness ratio and internally complex structures, such as missiles and launch vehicles, the interaction effects of elastic deformations on rigid motions are not negligible. In many studies, the rigid and elastic equations of motion are coherently derived following a Lagrangian approach [3-9]. Waszak and Schmidt [3] have obtained the elastic airplane equations of motion neglecting spherical and earth rotation, fluid motion and rotating mechanisms. Bilimoria [4] later modified their derivations for applications on a Single Stage To Orbit (SSTO) launch vehicle and verified the individual effect of the neglected terms in the trajectory and design optimization. Meirovitch [5] has also derived the Lagrange equations in terms of quasi-coordinates and quasi-moments [6], which includes the rigid mode effects.

Even though the elastic equations of motion have been extensively utilized in dynamic stability and trajectory evaluation of flexible spacecraft and missiles [7-9], most of the work in this area involves application of the linearized equations of motion.

Simulation of non-linear equations of an elastic missile, idealized as a uniform beam, has been performed for an uncontrolled missile [10], using flat earth assumption and linear aerodynamic theory, where the elastic bending and axial deformations are incorporated in the equations, following the method of assumed modes [10,11].

In the present study, the non-linear elastic equations of motion are derived for a controlled launch vehicle idealized as a variable mass, non-uniform beam, following the method of assumed modes and using Lagrange equations. This approach accounts for the inherent rigid-elastic modal interaction effects, as well as the control forces effect on the elastic properties. Various useful evaluations noted in this study include investigation of the effect of the IMU vibration, measuring devices optimum location, rotating machinery and structural damping on the vehicle trajectory and the required control action histories.

EQUATIONS OF MOTION

Representing linear and angular velocity vectors relative to inertial axes by $\vec{V}$ and $\vec{\omega}$, respectively, the linear and angular momentum of the vehicle can be written

*. *Corresponding Author, Department of Aerospace Engineering, Sharif University of Technology, Tehran, I.R. Iran.*

1. *Department of Aerospace Engineering, Sharif University of Technology, Tehran, I.R. Iran.*

as:

$$\vec{P} = \left(\frac{\partial T}{\partial \vec{V}}\right)^T, \tag{1}$$

$$\vec{h} = \left(\frac{\partial T}{\partial \vec{\omega}}\right)^T, \tag{2}$$

where T is the vehicle total kinetic energy.

The governing equations of motion in body axes are next represented by:

$$\vec{F}^B = \frac{d\vec{P}^B}{dt_I} = \frac{d\vec{P}^B}{dt_B} + \vec{\omega}^B_{IB} \times \vec{P}^B, \tag{3}$$

$$\vec{M}^B = \frac{d\vec{h}^B}{dt_I} = \frac{d\vec{h}^B}{dt_B} + \vec{\omega}^B_{IB} \times \vec{h}^B, \tag{4}$$

where the superscript B and d/dt_B denote the vector in the body axis and its time derivative relative to the body axis system, respectively. Similar co-notations are valid for I, where I stands for the inertial axis system. The external forces and moments exerted on the vehicle are denoted by $\vec{F}^B$ and $\vec{M}^B$, respectively. The form of the governing Equations 3 and 4 makes them readily adaptable to the standard Lagrange equation for elastic degrees of freedom in generalized coordinates (Equation 5):

$$\frac{d}{dt}\left(\frac{\partial T}{\partial \dot{\eta}_i}\right) - \frac{\partial T}{\partial \eta_i} + \frac{\partial U}{\partial \eta_i} + \frac{\partial D}{\partial \dot{\eta}_i} = Q_{\eta_i}, \tag{5}$$

where U and D are the potential and dissipative energy terms, respectively and Q_{η_i} represents the vector of generalized forces in η_i direction.

Vehicle Kinetic Energy

The kinetic energy of the missile is expressed as:

$$T = \frac{1}{2}\int \frac{d\vec{E}d\vec{E}}{dt_I dt_I} dm, \tag{6}$$

where $\vec{E}$ denotes the position of individual mass element dm relative to the inertial frame. Neglecting the vehicle axial deformation and assuming the lateral and transverse deflections, in terms of the natural bending modes of vibration, the vehicle local displacement vector, $\overline{e}$, can be written as [9-11]:

$$\vec{e}(x,t) = \begin{Bmatrix} 0 \\ \sum_{i=1}^{n} \eta_i(t)\phi_i(x) \\ \sum_{i=1}^{m} \zeta_i(t)\phi_i(x) \end{Bmatrix}, \tag{7}$$

where, due to the natural symmetry of the missile or launch vehicle, the modeshapes in the y and z directions have been assumed to be identical and equal to $\phi_i(x)$. Representing the position vector of each mass element, with respect to the center of mass of the dry (no fuel) vehicle, by $\vec{r}_0$, the instantaneous position of each mass element, relative to body ($\vec{r}$) and inertial frames, ($\overline{E}$), are related as shown in Figures 1 and 2:

$$\vec{r} = \vec{r}_0 + \vec{e}, \tag{8}$$

$$\vec{E} = \vec{R} + \vec{r}. \tag{9}$$

Expanding Equation 6 for the burning (m_g) and remaining vehicle mass (m_s) results in:

$$\begin{aligned} T =& \frac{1}{2}m_s V^2 + \vec{V}\int \frac{d\vec{r}}{dt_I} dm_s + \frac{1}{2}\int \frac{d\vec{r}d\vec{r}}{dt_I dt_I} dm_s \\ &+ \frac{1}{2}m_g V^2 + \vec{V}\int \frac{d\vec{r}}{dt_I} dm_g + \frac{1}{2}\int \frac{d\vec{r}d\vec{r}}{dt_I dt_I} dm_g. \end{aligned} \tag{10}$$

where the fourth term in the above equation is assumed negligible in comparison with the first term ($m_g <<$

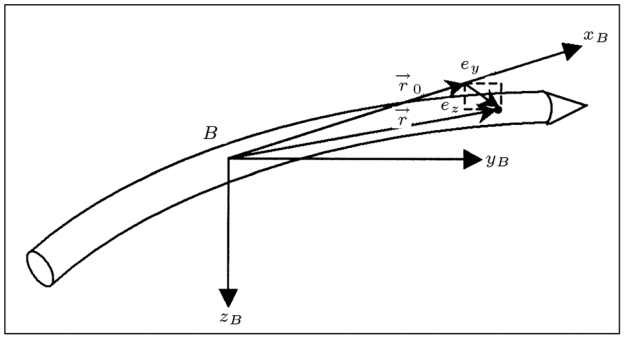

Figure 1. Missile in the bending position.

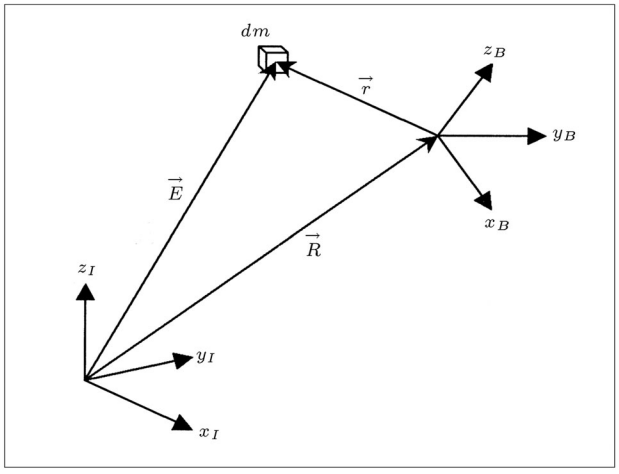

Figure 2. Position of mass element.

m_s). Also, the fifth term is approximated as:

$$\vec{V}\int \frac{d\vec{r}}{dt_I}dm_g = -\dot{m}X_{\text{out}}U, \tag{11}$$

where X_{out} is the distance from the hot gases exit plane to the burning area, $\dot{m}$ the fuel and oxidizer mass flow rate and U represents the axial velocity component of $\vec{V}$ in the body axes system. In addition, the last term of Equation 10 is due to thrust action that would not appear in the final equations, as a result of the expansion of Equation 1 through Equation 4. Therefore, the thrust force is modeled as an external force. The vehicle total kinetic energy can now be expressed as:

$$\begin{aligned} T =& \frac{1}{2}m_s(U^2+V^2+W^2) - \dot{m}X_{\text{out}}U + \frac{1}{2}P^2I_x \\ &+\frac{1}{2}(Q^2+R^2)I+\frac{1}{2}P^2\sum_{i=1}^{n}(\zeta_i^2+\eta_i^2) \\ &+p\sum_{i=1}^{n}(\eta_i\dot{\zeta}_i-\zeta_i\dot{\eta}_i)+\frac{1}{2}\sum_{i=1}^{n}(\dot{\eta}_i^2+\zeta_i^2)+\frac{1}{2}Q^2\sum_{i=1}^{n}\zeta_i^2 \\ &+\frac{1}{2}R^2\sum_{i=1}^{n}\eta_i^2 - QR\sum_{i=1}^{n}\eta_i\zeta_i. \end{aligned} \tag{12}$$

It needs to be mentioned that the orthogonality assumption of elastic modes has been assumed in the derivation of Equation 12, namely:

$$\int \phi_i(x)dm_s = \int x\phi_i(x)dm_s = 0, \tag{13}$$

$$\int \phi_i(x)\phi_j(x)dm_s = \begin{cases} 0 & i=j \\ 0 & i\neq j \end{cases}. \tag{14}$$

Potential Energy

In the present form of the rigid equations of motion (Equations 1 to 4), gravity is taken as an external force acting on the vehicle, thus, it should not be a part of the potential energy relation. Therefore, only the elastic strain energy is considered in Equation 5, which is expressed in terms of elastic displacements:

$$U = \int_0^L EI\left[\left(\frac{\partial^2 e_y}{\partial x^2}\right)^2 + \left(\frac{\partial^2 e_z}{\partial x^2}\right)^2\right]dx. \tag{15}$$

The governing differential equation of the elastic bending modeshapes, in the absence of axial force effects, is utilized for computation of the shape functions, ϕ_i:

$$\frac{d^2}{dx^2}\left(EI\frac{d^2\phi_i}{dx^2}\right) - \omega_i^2\rho A\phi_i(x) = 0, \tag{16}$$

where ρA represents the vehicle mass density per unit length. Subsequently, the elastic potential energy part of Equation 15 can be determined in terms of quasi-coordinates, η_i, ζ_i and modal natural frequencies, ω_i, as:

$$U = \frac{1}{2}\sum_{i=1}^{n}(\eta_i^2+\zeta_i^2)\omega_i^2. \tag{17}$$

Dissipative Energy

Using the conventional model of dissipative energy [9],

$$D = \frac{1}{2}\int c\left[\left(\frac{de_y}{dt}\right)^2 + \left(\frac{de_z}{dt}\right)^2\right]dx, \tag{18}$$

where $c = 2\mu_i\omega_i$ and μ_i denotes the critical damping ratio of the ith bending mode. One can arrive at the following form of damping energy, to be used in Equation 5:

$$D = \sum_{i=1}^{n}\mu_i\omega_i(\dot{\eta}_i^2+\dot{\zeta}_i^2). \tag{19}$$

Finally, through substitution of Equations 12, 17 and 19 in Equations 1 to 5, the joint rigid and elastic nonlinear equations of motion are arrived at:

$$\dot{U} = \frac{F_X}{m_s} + RV - QW, \tag{20}$$

$$\dot{V} = \frac{1}{m_s}(F_y + \dot{m}X_{\text{out}}R) + PW - RU, \tag{21}$$

$$\dot{W} = \frac{1}{m_s}(F_z - \dot{m}X_{\text{out}}Q) + QU - PV, \tag{22}$$

$$\begin{aligned} \dot{P} =& \frac{1}{I_x+\Sigma(\eta_i^2+\zeta_i^2)}\Big[M_x - \Sigma(\eta_i\ddot{\zeta}_i - \ddot{\eta}_i\zeta_i) \\ &- 2P\Sigma(\zeta_i\dot{\zeta}_i+\eta_i\dot{\eta}_i)(Q^2-R^2)\Sigma\eta_i\zeta_i + \\ &+ QR\Sigma(\zeta_i^2-\eta_i^2)\Big], \end{aligned} \tag{23}$$

$$\begin{aligned} \dot{Q} =& \frac{1}{I+\Sigma\zeta_i^2}\Big[M_y + PR(I-I_x) - PR\Sigma\zeta_i^2 \\ &+ (\dot{R}-PQ)\Sigma\eta_i\zeta_i + 2R\Sigma\zeta_i\dot{\eta}_i - 2Q\Sigma\zeta_i\dot{\zeta}_i\Big], \end{aligned} \tag{24}$$

$$\begin{aligned} \dot{R} =& \frac{1}{I+\Sigma\eta_i^2}\Big[M_z + PQ(I_x-I) + PQ\Sigma\eta_i^2 \\ &+ (\dot{Q}+PR)\Sigma\eta_i\zeta_i + 2Q\Sigma\eta_i\dot{\zeta}_i - 2R\Sigma\eta_i\dot{\eta}\Big], \end{aligned} \tag{25}$$

$$\begin{aligned} \ddot{\eta}_i =& Q_{\eta_i} - 2\mu_i\omega_i\dot{\eta}_i + (P^2+R^2-\omega_i^2)\eta_i \\ &+ 2P\dot{\zeta}_i + (-QR+\dot{P})\zeta_i, \end{aligned} \tag{26}$$

$$\ddot{\zeta}_i = Q_{\zeta_i} - 2\mu_i\omega_i\dot{\zeta}_i + (P^2 + Q^2 - \omega_i^2)\zeta_i$$

$$- 2P\dot{\eta}_i - (\dot{P} + QR)\eta_i. \quad (27)$$

As noted from the above equations, the last two differential equations are of 2nd order, which through definitions of auxiliary state variables, $\dot{\zeta}_i$ and $\dot{\eta}_i$, should be put into the required state space format.

GUIDANCE AND CONTROL

For this study, a simple three axes Inertial Navigation System (INS) was utilized.

Guidance Law

A proven guidance scheme for the powered phase of launcher applications could be based on the idea of the required velocity. The required velocity, $(\vec{V}_R)$, is defined as the burn-out velocity, which would provide the desired range when flown ballistically. Most guidance routines, however, use the difference of this velocity and the missile instantaneous velocity, $(\vec{V})$, to come up with the required control scheme:

$$\vec{V}_g = \vec{V}_R - \vec{V}, \quad (28)$$

where $\vec{V}_g$ is the so called velocity to be gained. Explicit methods for finding $\vec{V}_g$ involve instantaneous computation of $\vec{V}_R$ and use of Equation 28, while implicit methods utilize a differential equation for the computation of the velocity to be gained. This equation is obtained assuming $\vec{V}_g$ to be only functions of time and position in flight and that only the gravitational force is acting on the vehicle after burn-out. This differential equation, in an inertial frame, is written as [12]:

$$\dot{\vec{V}}_g^I = -Q\vec{V}_g^I - \vec{a}_T^I, \quad (29)$$

where, $\vec{a}_T^I$ is the vector of non-gravitational accelerations in inertial frame and the Q matrix is defined as follows:

$$Q \triangleq \frac{\partial \vec{V}_R^I}{\partial \vec{r}^I}. \quad (30)$$

One can determine the Q matrix for various trajectories through the numerical solution of the Lambert problem [12,13]. Results show that for short to medium ranges, Q can effectively be a function of time. For Strap-down INS systems, Equation 29 would be written in a body axes system:

$$\dot{\vec{V}}_g^B = -Q^*\vec{V}_g^B - \vec{a}_T^B, \quad (31)$$

where Q^* is now defined as:

$$Q^* = [DCM]^{BI} Q [DCM]^{IB} + \Omega_B, \quad (32)$$

and $[DCM]^{BI}$ and $[DCM]^{IB}$ are the inertial to body and body to inertial transformation matrices, respectively. Also, Ω_B, the cross-product matrix corresponding to the operator $(\omega_{IB}^B\times)$, can be found from the following relation:

$$\Omega_B = -(\Omega_B)^T = [\omega_{IB}^B\times] = \begin{bmatrix} 0 & -R & Q \\ R & 0 & -P \\ -Q & P & 0 \end{bmatrix}. \quad (33)$$

In the above equation, P, Q and R are the vehicle angular velocity $(\vec{\omega}_{BI}^B)$ components coming out of the strapped-down gyro's of the INS.

Command Laws

The purpose of the guidance and control system for the method chosen is to zero-out the velocity to be gained, $\vec{V}_g$. This can be done through accelerating in the direction of $\vec{V}_g$. As a result, the command angular velocities for controls are determined using the method of cross product steering [14]:

$$\vec{\omega}_c^B = k\frac{\vec{a}_T^B \times \vec{V}_g^B}{a_T V_g}, \quad (34)$$

where k is a function of burn-out condition denoted by (T_{go}), which can be approximated by V_g/a_T.

Control System Commands

The vehicle is to be controlled via internal control surfaces. A displacement type autopilot is considered, which requires conversion of the angular velocity commands to the required angular displacement commands.

VEHICLE FORCES

The vehicle forces and moments are due to aerodynamics, exhaust gases and gravity. The generalized distributive and concentrated forces, using the principle of virtual work, are derivable from the following relations:

$$Q_{\eta_i}(t) = \int_0^L f_y(x,t)\phi_i(x)dx, \quad (35)$$

$$Q_{\eta_i}(t) = F_y(t)\phi_i(x_1), \quad (36)$$

where similar equations are also derivable for Q_{ζ_i}.

Gravitational Force

The gravitational force for an elliptic earth model is obtained as a function of position ($\vec{E}$). However, as a result of Equation 13, there would be no gravity contribution for the generalized forces.

Aerodynamic Forces

Vehicle aerodynamic force and moment coefficients per unit length are determined either from engineering codes in table look-up form or by using the results of wind-tunnel experiments as a function of angle of attack, sideslip, Mach and Reynold's number. Due to a vehicle's local bending deflections, the vehicle's local (elemental) angles of attack and sideslip are determined from the following quasi-static relations:

$$\alpha(x,t) = \tan^{-1}\left(\frac{W_\infty}{U_\infty}\right) + \frac{\dot{e}_z(x)}{U_\infty} + \frac{Pe_y(x)}{U_\infty} + \frac{Qx}{U_\infty} - e'_z(x), \tag{37}$$

$$\beta(x,t) = \tan^{-1}\left(\frac{V_\infty}{U_\infty}\right) + \frac{\dot{e}_y(x)}{U_\infty} - \frac{Pe_z(x)}{U_\infty} + \frac{Rx}{U_\infty} - e'_y(x), \tag{38}$$

where U_∞, V_∞ and W_∞ are the vehicle's velocity ($\vec{V}$) components in body coordinates. The aerodynamic forces and moments per unit length are evaluated as:

$$f = q_\infty S_{ref} \overline{C}_f, \tag{39}$$

$$m = q_\infty S_{ref} L_{ref} \overline{C}_m, \tag{40}$$

where S_{ref} is the reference area based on the vehicle's maximum diameter, also, $\overline{C}_f$ and $\overline{C}_m$ are the aerodynamic force and moments coefficients per unit length.

Exhaust Forces

Exhaust forces include thrust and control action forces, considered externally acting on the vehicle. These forces are determined in a local body axes adjacent to the exhaust plane and are next transformed into the vehicle body axes, considering any local bending or misalignments.

SIMULATION PROGRAM

A complete simulation program has been developed in the C^{++} environment. The vehicle non-linear equations of motion are time integrated using a fourth order forward Runge-Kutta algorithm. The aeroelastic simulation routine proved to be an invaluable tool for design evaluation and optimization of flexible guided vehicles. An inherent modular structure of the program allows for different modelling of the guidance and control algorithm, aerodynamics load prediction routines and beam models.

RESULTS

One of the main goals of aeroelastic analysis is to evaluate the feasibility of optimized new designs through investigation of the influence of the key parameter on vehicle performance, stability and control during flight. In this regard, the key influencing parameters have been selected as equivalent bending stiffness, local vibrational forcing, vibrational effect of measuring devices and their location and structural damping. During the analysis, it was noted that for the configuration under study, aerodynamic loadings mainly cause quasi-static displacements and, because of the form of aerodynamic pressure distribution, these forces excite the vehicle's fundamental mode of vibration. Similarly, the control forces primarily excited the first vehicle mode. Therefore, based on the results and previous work [10,11], the first three modes of vibration have been utilized and considered sufficient for modelling the vehicle elastic bending deflections.

Bending Stiffness

Obviously, reduction of bending stiffness increases total displacements, as noted in Figure 3, which shows the missile's elastic displacements at the exhaust plane. Figure 4 shows the control surface deflections for various missiles' equivalent bending stiffness. It can be seen from the results that the control efforts can either increase or decrease, depending on the missile's displacements at the exhaust plane. As shown in Figure 3b, the missile's end deflection is positive for about 40% of the total time. Accordingly, Figure 4b shows a reduction of control movements with a decrease of bending stiffness in the same time span. This result is mainly due to aerodynamic loading effect causing displacements, since no exciting forces have yet been considered. Also, results indicate that there exists a minimum level of bending stiffness, below which structural divergence occurs. This, in part, is due to the fact that a reduction of stiffness causes additional displacements, due to aerodynamic forces, which, in turn, increases aerodynamic forces. Obviously, this process leads to static instability.

Vibration of the Measuring Devices

The following equation relates the origin of the body axes system to the measuring devices (IMU) location:

$$\vec{R}_U^B = \vec{R}_B^B + \vec{R}_{UB}^B, \tag{41}$$

where $\vec{R}_B^B$ represents the position of the origin of the vehicle body axes relative to the inertial frame written in body coordinates, $\vec{R}_U^B$ represents the IMU position in body coordinates $\vec{R}_{UB}^B = \begin{bmatrix} X_U & e_{y_U} & e_{z_U} \end{bmatrix}^T$ and X_U is

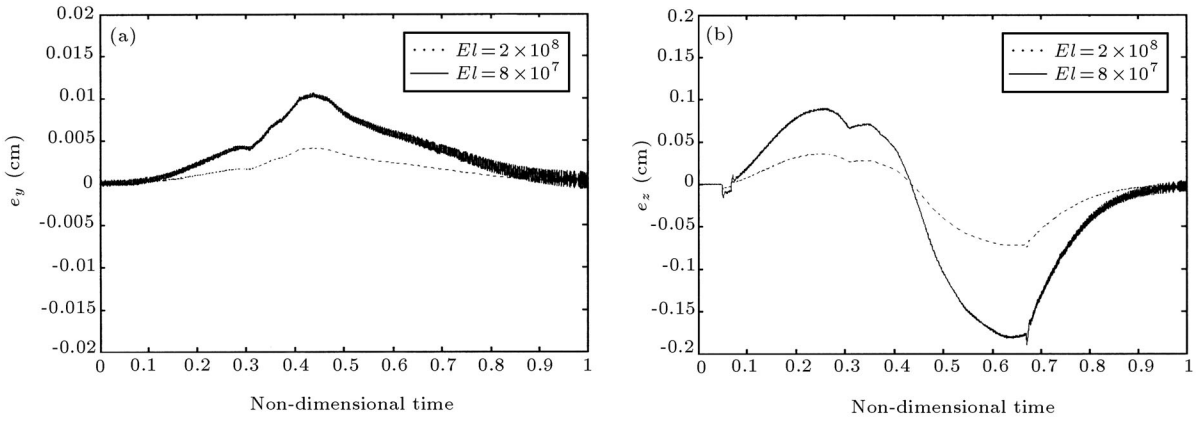

Figure 3. Equivalent stiffness effect on the elastic deformations at the vehicle exhaust plane.

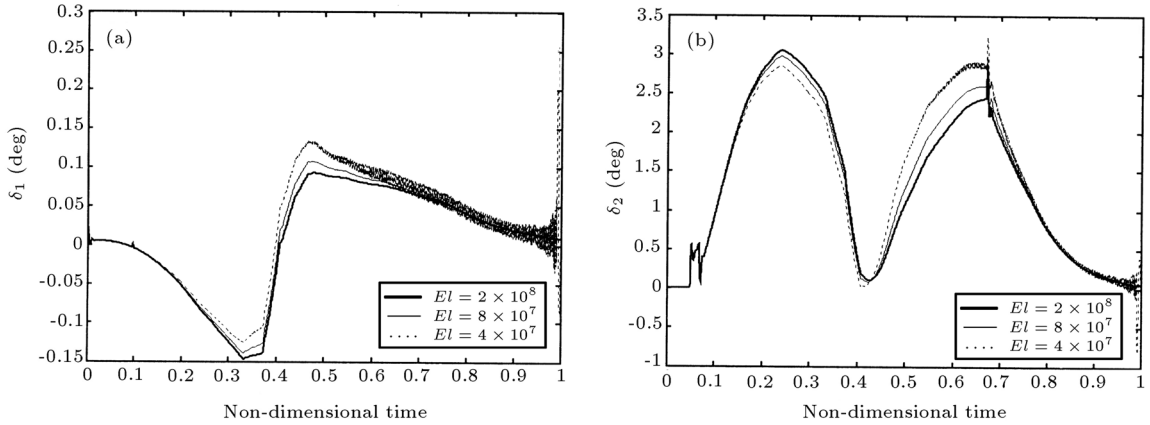

Figure 4. Equivalent stiffness effect on the control surface deflections.

the axial distance of the IMU to the origin of the body axes system (assuming IMU is on the missile center line). Using the above relations, one can compute the relative acceleration of the IMU, with respect to the center of the body axis system:

$$\frac{d^2\vec{R}^B_{UB}}{d^2t_I} = \frac{d^2\vec{R}^B_{UB}}{d^2t_B} + \frac{d\vec{\omega}^B_{IB}}{dt_B} \times \vec{R}^B_{UB} + 2\vec{\omega}^B_{IB} \times \frac{d\vec{R}^B_{UB}}{dt_B} + \vec{\omega}^B_{IB} \times (\vec{\omega}^B_{IB} \times \vec{R}^B_{UB}). \quad (42)$$

Also, the relative IMU angular velocity, with respect to the body axes due to gyros vibrational effect, could be expressed as:

$$q_{UB} = -\frac{\partial}{\partial t_B}(\frac{\partial e_{z_U}}{\partial x}) = -\frac{\partial}{\partial x}(\frac{\partial e_{z_U}}{\partial t_B}), \quad (43)$$

$$r_{UB} = \frac{\partial}{\partial t_B}(\frac{\partial e_{y_U}}{\partial x}) = \frac{\partial}{\partial x}(\frac{\partial e_{y_U}}{\partial t_B}). \quad (44)$$

The above components contributing to the linear accelerations and angular velocities (due to the vibrational effect of the IMU) are, subsequently, added to the pertinent terms in the equations of motion. Depending on the assumed IMU location, this effect could be of varying importance and it can even destabilize the missile. Also, inclusion of these contributing terms plays a crucial role in vehicle vibrational behavior, once vibrational excitive forces are additionally introduced in the simulation.

Forcing Functions

Many sources of forced excitations could be present during the actual flight of a launch vehicle. Among the more important sources are: Unsteady aerodynamic loading, engine thrust fluctuations, vibrational effect of rotating machinery and atmospheric turbulence. The inherent nature of these forces could either be deterministic or random. The main source of external random disturbance is due to atmospheric turbulence, for which various models exist. However, due to the broad frequency spectrum of the white noise source generating these signals through appropriate shaping filters, they are not considered potentially critical and do not create any significant vibratory response characteristics.

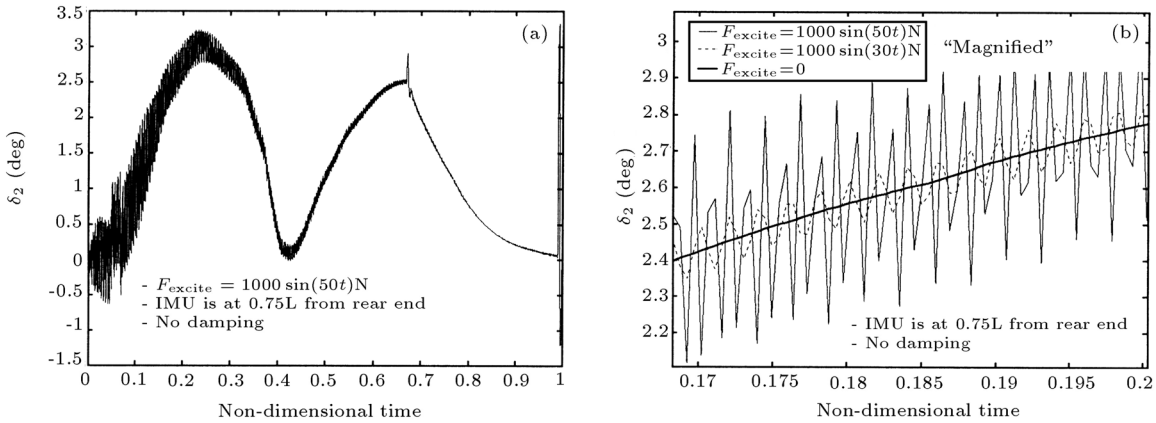

Figure 5. Excitation forces effect on the control deflection.

On the other hand, some of the internal system components and mechanisms, such as rotating turbomachinary, gyro rotors and etc. acting as internal disturbing forcings, posses frequency contents with prevailing conspicuous magnitudes of importance. And, since one of the key issues of interest in this article has been to examine structure/system interactional effects, it is quite justifiable to apply sinusoidal forcing functions with frequency near working/natural frequencies of the system under study. Thus, the following harmonic forcing function is utilized for the purpose of parametric investigation:

$$F_{\text{excite}} = A\sin(\omega t + \varphi). \tag{45}$$

The amplitude, frequency and application point of this force on the vehicle is of importance. Due to the relative high frequency nature of the actual forcing functions present in flight, their significant effect would only be on the elastic deformations (Equation 36) and they do not seem to directly influence vehicle dynamics. In the case studied here, the application point of this force is selected at 84% from the vehicle nose. This location corresponds to the engine support/attachment mechanism through which engine induced excitations are transmitted to the structure. Results indicate a greater role for the influence of frequency compared with amplitude. Figure 5 shows that increasing the forcing frequency, close to the fundamental natural frequency of the structure (about 60 rad/sec at the beginning of flight), causes an increase in structural vibrations. Thus, even though the excitive force amplitude is very small to motivate structural vibrations, the oscillatory control actions (due to IMU vibrations) cause structural oscillations, which, in turn, cause additional control vibrations and so on. The control vibratory actions eventually subside, due to an increase in vehicle fundamental natural frequency, as a result of burning fuel and subsequent mass reduction (Figure 5a).

Structural Damping

Large forcing functions introduced through Equation 45 will obviously develop large oscillatory deformations leading to divergence. Preventive measures can be applied in two forms, addition or increase of structural damping and filtering elastic vibrations out of the measuring devices output (IMU) and noise. Both schemes have shown to be effective. An increase in the structural damping coefficient reduces the amplitude of the control action fluctuations. Also, filtering out the vibrations from the measuring devices output produces more acceptable vehicle dynamics, as evidenced in Figure 6. Figure 5a presents the variation of a control deflection, due to a sinusoidal forcing, for the whole time span of controlled motion. It is assumed that the filter is ideal, thus, the IMU only measures the rigid body dynamic characteristics. A typical forcing function, F = 1000 sin(60t), is used for the analysis and, as expected, without filtering the IMU outputs, the system initially becomes highly oscillatory. Since the amplitude of the forcing function is not relatively large, it is concluded that the resulting behavior is largely due to the passage of raw IMU

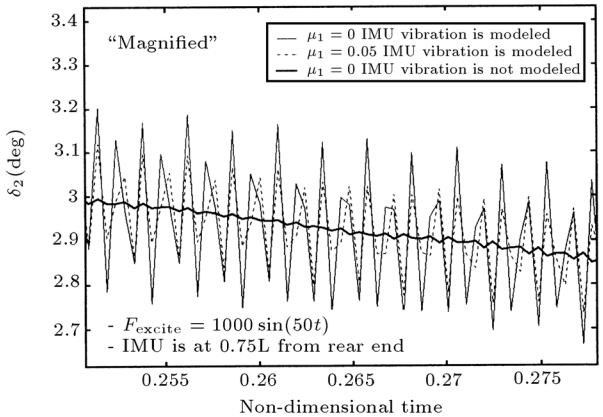

Figure 6. Effect of the first mode damping on the control deflection.

information to the guidance and control logic, resulting in large control forces. In turn, the large control forces intensify structural excitations that might lead the system to divergence. As mentioned earlier, a local damping mechanism and/or an appropriate low pass pre-filter could be used in order to prevent system instability during large amplitude high frequency forcing. It needs to be mentioned that the usual noise filters (in measuring systems) usually prevent the low amplitude, high frequency oscillations from entering the control and guidance routines, while large period vibrations can also have severe adverse effects on vehicle performance and its subsequent orbital injections.

Guidance Unit Effects

A passive method for the reduction of the IMU vibrational effects is to determine an optimal location for its installation. This could be a position of minimum vibration on the vehicle longitudinal axes. By inspection of the vehicles bending deflections in time, it is realized that a typical launcher body often takes the form of its first (primary) mode and that only two nodes develop. These nodes behave in a quasi-static fashion and have very little movement as higher modes are excited in flight. Even though these nodes could be ideal locations for sensors measuring acceleration, they would not be as appropriate for the other sensors. Figure 7 shows the beneficial effect of the IMU location on the vehicle accelerations. For this analysis, the IMU was located at 0.35 L from the vehicle nose. Since this position may not be ideal for installation of gyros (Figure 8), a compromise is usually required to determine an optimum IMU location resulting in a minimum oscillatory control action (Figure 9) during flight. For a uniform model, an inherently ideal position for the IMU, in view of angular rates, is at 0.5 L, but the numerical investigation for a non-uniform model indicated a modified IMU position at 0.45 L to be appropriate, both in terms of angular rates as well as control actions. Also, the analysis showed that for the system under study, the IMU location in the aft portion of vehicle ($X_U > 0.5$ L) could lead to dynamic instability. Of course, this problem could be overcome if

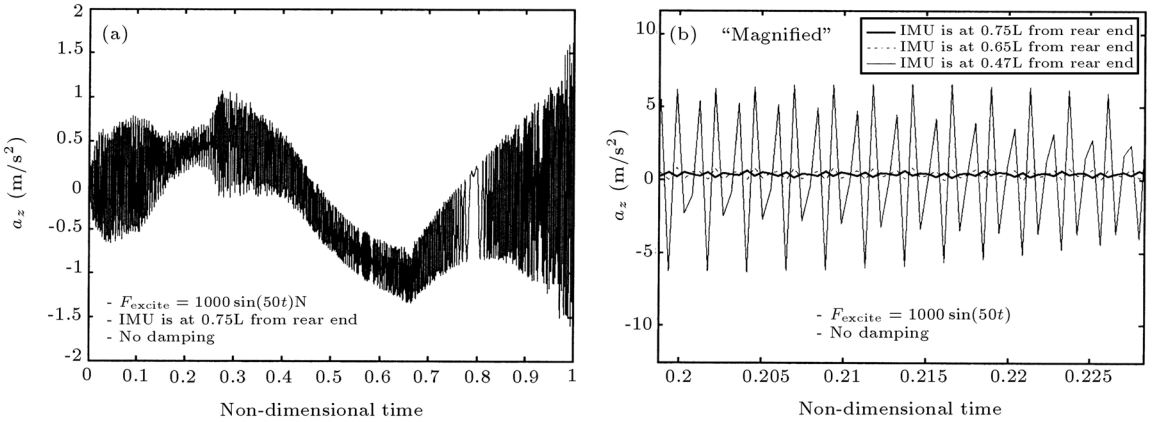

Figure 7. Effect of the IMU location on the output of accelerometers (z direction).

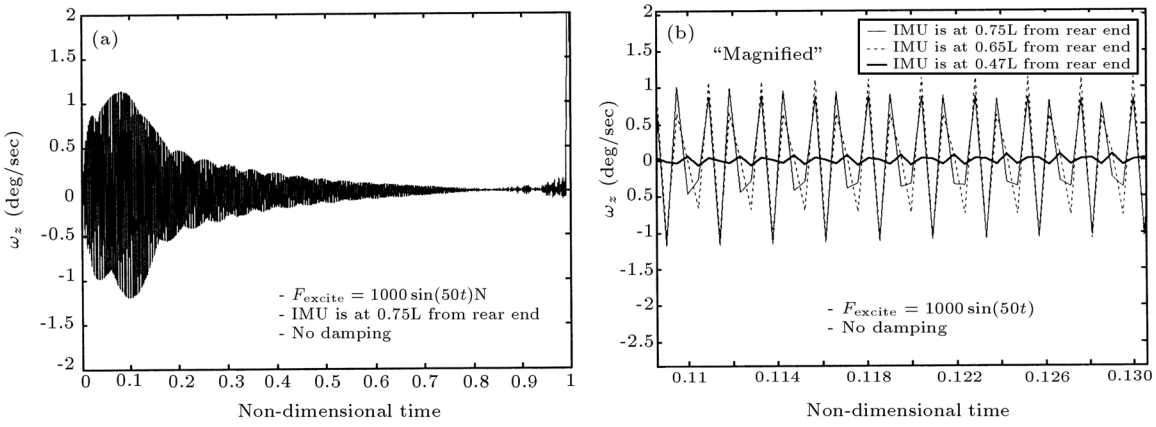

Figure 8. Effect of the IMU location on the output of gyros (about z axis).

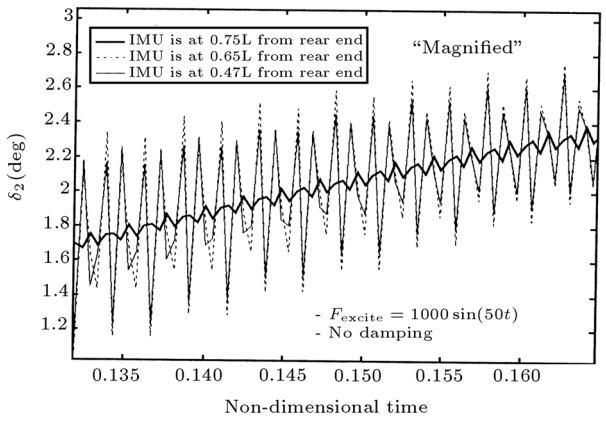

Figure 9. Effect of the IMU location on the control deflection.

the control system were redesigned considering elastic effects.

The Generalized Coordinates

These coordinate are directly used to determine the vehicle's deformed shapes through Equation 7. By investigation of their time history, one can detect the relative importance of the higher modes (order of magnitude comparison) or the sensitive times when higher modes are excited. This information, plus the temporal distribution of bending deflections (in two directions) at various locations, is useful for many design oriented applications and/or optimizations. Figure 10 shows typical variations of these coordinates for the first three modes without excitations or damping. As can be seen, the second and third mode coefficients are of considerably smaller magnitude as compared with the first. Thus, selection of three modes for this analysis is appropriate.

CONCLUDING REMARKS

Aeroelastic analysis of a guided launch vehicle has been performed on the basis of coupled, non-linear, rigid-elastic equations of motion. The developed methodology allows for the study of aeroelastic bending effects on the dynamic stability and control of a launch vehicle with rigid-elastic-control interactions accounted for. Results indicate the high sensitivity of the vehicle to forced excitations, which must be properly handled to avoid control saturation and/or structural instability. The influence of various design and optimization parameters, such as reduced local stiffness, structural damping and the location of measuring devices on vehicle trajectory and control, have also been investigated. It was also found that an IMU location in the aft portion of the vehicle could lead to dynamic instability.

NOMENCLATURE

$\vec{V}$	velocity vector
$\vec{\omega}$	angular velocity vector
$\vec{P}$	linear momentum
$\vec{h}$	angular momentum
T	vehicle total kinetic energy
$\vec{F}$	external forces
$\vec{M}$	external moments
U	potential energy
D	damping energy
η_i, ζ_i	ith mode generalized coordinates
$\phi_i(x)$	ith modeshape
ω_i	ith mode natural frequency
Q_{η_i}, Q_{ζ_i}	ith mode generalized forces
$\vec{R}$	position vector of the center of mass relative to inertial frame
$\vec{E}$	position vector of the individual mass element dm relative to inertial frame
$\vec{r}$	position vector of the individual deformed mass element dm relative to body frame
$\vec{r}_0$	position vector of the individual undeformed mass element dm relative to body frame
$\vec{e}$	vehicle local displacement vector
m_s	vehicle structural mass
m_g	burning mass
X_{out}	distance from the hot gases exit plane to the burning area
$\dot{m}$	fuel and oxidizer mass flow rate
ρA	vehicle mass density per unit length
EI	vehicle bending rigidity
μ_i	critical damping ratio
$\vec{V}_R$	required velocity
$\vec{V}_g$	velocity to be gained
$\vec{a}_T$	vehicle non-gravitational acceleration vector
Q, Q^*	guidance matrices
$[DCM]^{BI}$	direction cosine matrix from I to B
Ω_B	cross-product matrix corresponding to the operator $(\omega^B_{IB}\times)$
$\vec{\omega}_c$	rate command
$\alpha(x,t)$	local angle of attack
$\beta(x,t)$	local angle of sideslip
q_∞	dynamic pressure

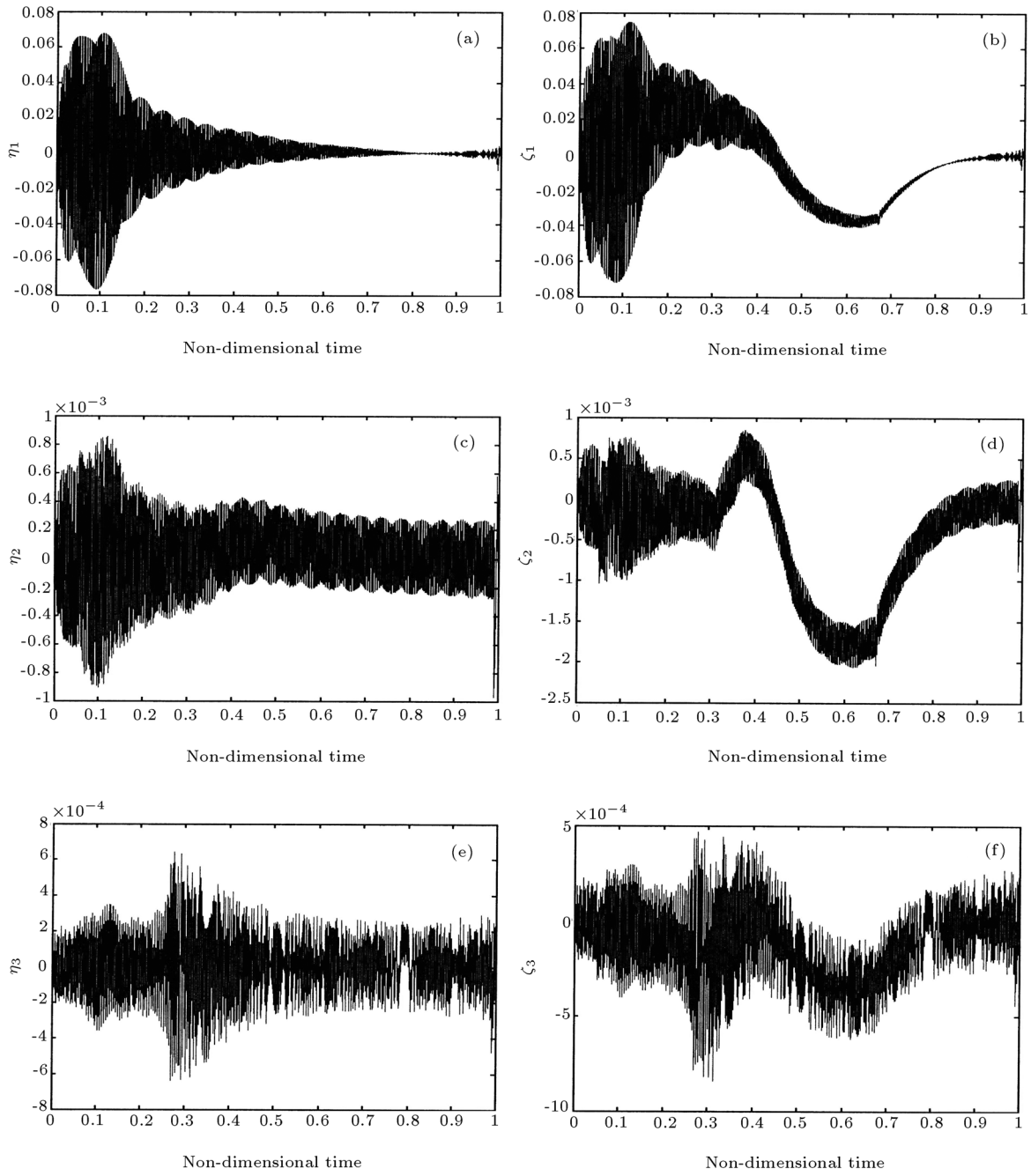

Figure 10. Temporal behavior of the generalized coordinates ($F_{\text{excite}} = 1000\sin(50t)N$–IMU is at 0.75 L from rear end - no damping).

S_{ref}	reference area
L_{ref}	reference length
$\overline{C}_f, \overline{C}_m$	aerodynamic force and moments coefficients per unit length
F_{excite}	harmonic exciting force
$\dfrac{d}{dt_I}$	time derivative relative to inertial axes system
$\dfrac{d}{dt_B}$	time derivative relative to body axes system
$\vec{R}^B_{UB} = [X_U \;\; e_{yU} \;\; e_{zU}]^T$	distance between the IMU location to the origin of the body axes

Superscript

I	expression of the vector in inertial axes system

B expression of the vector in body axes system

REFERENCES

1. Blackelock, J.H., *Automatic Control of Aircraft and Missiles*, John Wiley & Sons, NewYork, USA (1992).
2. Bisplinghoff, R.L. and Ashley, H. *Principles of Aeroelasticity*, Dover Publication, NY, USA (1975).
3. Wasak, M.R. and Schmidt, D.K. "Flight dynamics of aeroelastic vehicles", *Journal of Aircraft*, **25**(6), pp 563-571 (1988).
4. Bilimoria, K.D. "Integrated development of the equations of motion for elastic hypersonic flight vehicle", *Journal of Guidance,Control and Dynamics*, **18**(1), pp 73-81 (1995).
5. Meirovitch, L. "Hybrid state equation of motion for flexible bodies in terms of Quasi-Coordinates", *Journal of Guidance, Control and Dynamics*, **14**(5), pp 1008-1013 (1991).
6. Meirovetch, L. "State equations for maneuvering and control of flexible bodies using quasimomenta", *Journal of Guidance, Control and Dynamics*, **16**(5), pp 882-891 (1993).
7. Meirovitch, L. and Nelson, H.D. "On the high-spin motion of a satellite containing elastic parts", *Journal of Spacecraft and Rockets*, **3**(5), pp 1597-1602 (Nov. 1966).
8. Crimi, P. "Aeroelastic stability and response of flexible tactical weapons", *AIAA*, pp 84-0392 (Jan. 1984).
9. Platus, D.H. "Aeroelastic stability of slender, spinning missiles", *Journal of Guidance, Control and Dynamics*, **15**(1), pp 144-151 (1990).
10. Ghamkhar, A.R. and Salehzadeh, A. "Investigation of the aeroelasticity effect on a typical ballistic missile", M.S. Project, Department of Aerospace Engineering, Amir Kabir University (1999).
11. Shafinaderi, A.A., Kabganian, M. and Alasty, A. "Influence of flexibility on missile dynamic behavior", M.S. Project, Department of Aerospace Engineering, Amir Kabir University (1999).
12. Battin, R.H. "An introduction to mathematics and methods of astronautics", *Education Series, AIAA*, New York, USA (1987).
13. Battin, R.H. "Solution of the Lambert's Problem with Gauss Method", *Journal of Guidance, Control and Dynamics*, **2**(3), pp 190-195 (1979).
14. Pitman, G.R., *Inertial Guidance*, John-Wiley & Sons (1962).